Eur. Phys. J. Appl. Phys. **46**, 30901 (2009)
DOI: 10.1051/epjap/2009067

THE EUROPEAN PHYSICAL JOURNAL APPLIED PHYSICS

Regular Article

Characterization of tracks in CR-39 detectors obtained as a result of Pd/D Co-deposition

P.A. Mosier-Boss[1,a], S. Szpak[1], F.E. Gordon[1], and L.P.G. Forsley[2]

[1] SPAWAR Systems Center Pacific, Code 7173, San Diego, CA 92152, USA
[2] JWK International Corp., Annandale, VA 22003, USA

Received: 15 January 2009 / Accepted: 5 March 2009
Published online: 17 April 2009 –

Abstract. Earlier we reported that the pits generated in CR-39 detectors during Pd/D co-deposition experiments are consistent with those observed for pits that are of a nuclear origin. Spacer experiments and track modeling have been done to characterize the properties of the particles that generated the tracks in the CR-39 detectors. The effect of water on the energetics of the particles and their resultant tracks is discussed.

PACS. 29.30.Ep Charged-particle spectroscopy – 29.40.Wk Solid-state detectors

1 Introduction

CR-39 is an allyl glycol carbonate plastic that has been widely used as a passive, limited spectral resolution, solid state nuclear track detector (SSNTD) in inertial-confinement-fusion (ICF) research [1]. The same attributes that make CR-39 detectors ideal for ICF experiments also make them attractive for use in Pd/D experiments. Specifically, CR-39 is inexpensive and robust. It interacts with both charged particles and neutrons and is insensitive to gamma and beta radiation as well as electromagnetic noise [1,2]. Consequently, CR-39 detectors can be placed close to a source without being damaged. Like photographic film, CR-39 is an example of an integrating detector. When an event occurs, it is permanently stamped in the plastic. The advantages of an integrating detector are (i) nothing gets lost or averaged away, (ii) the spatial distribution of the events can be determined, and (iii) the signal in the detector does not degrade with time. The first two attributes are particularly advantageous in experiments where emissions occur sporadically or at low fluxes. Such behavior has been reported for other nuclear emanations observed in the Pd/D system [3–6]. From the observed spatial distribution of the pits, the source of the emissions can be determined. The density of the pits can be used to determine the activity of a given site. The fact that the detector can be archived is advantageous in that the detector can be re-analyzed at a later date as improved read-out systems become available or to simply re-examine the detector to look for tracks that are diagnostic of a particular nuclear interaction. For example, triple tracks in which the individual lobes of the track are splitting from a center point are diagnostic of the $^{12}C(n,n')3\alpha$ carbon breakup reaction [7–12]. The main disadvantage of constantly integrating detectors is that it is not known when the events occurred. A recent review article does an in-depth discussion on the strengths and weaknesses of SSNTDs [13].

CR-39 has been used by several investigators to detect energetic particles in Pd/D electrolysis experiments [14–18]. Although different experimental configurations were used in these electrolysis experiments, they gave similar results. In the experiments done by Oriani and Fisher [14], CR-39 detectors were placed above and below Pd sheet cathodes. Since charged particles cannot travel far in water, this experimental configuration is not optimum for charged particle detection. Despite this, the track densities in their electrolysis experiments (150–3760 tracks cm^{-2}) were significantly higher that the track densities of the controls (59–541 tracks cm^{-2}). Lipson et al. [15] electrochemically loaded Au/Pd/PdO heterostructures with deuterium. Once loaded, the Au/Pd/PdO cathode was taken out of the cell and was tightly fixed on the surface of a CR-39 detector. The cathode attached to the detector was then subjected to temperature cycling between room temperature and 323 K for 1 h. After etching, tracks consistent for 2.5–3.0 MeV protons and 0.5–1.5 MeV tritons were observed in the detector. In another series of experiments, Lipson et al. [16,17] conducted in-situ measurements of energetic particles during the electrochemical loading of flat-plate Pd-thin film cathodes in light water. In these experiments, thin Pd films were placed in direct contact with

[a] e-mail: pam.boss@navy.mil

CR-39 detectors during electrolysis. Analysis of the CR-39 detectors showed the presence of tracks due to charged particles that were concentrated in areas where the cathodes were in contact with the detectors. The distribution of tracks was inhomogeneous indicating that some sites exhibit greater activity than others. Additional experiments were conducted by placing thin Cu and Al foils between the Pd cathode and the CR-39 detectors [17]. The purpose of these experiments was to differentiate between alpha particles and protons and to determine their energies. These experiments showed that the Pd cathodes emitted 11–16 MeV alpha particles and 1.7 MeV protons during electrolysis. In-situ electrolysis experiments were done using Pd wires in contact with CR-39 detectors [18]. Like the earlier Pd foil experiments done by Lipson et al. [16,17], tracks in the detectors in contact with the Pd wire were not homogeneously distributed over the length of the wire. This indicates that some areas in the bulk Pd are more active. It should be noted that, for bulk Pd, generation of heat, tritium, and helium does not occur homogeneously throughout the Pd [19].

More recently, CR-39 detectors have been used to detect charged particle emission during Pd/D co-deposition [18]. In these experiments, a non-hydriding cathode substrate, such as Au, Pt, or Ag wire, is placed in direct contact with a CR-39 detector. The cathode is then placed in a solution of $PdCl_2$ and LiCl in D_2O. When cathodically polarized, Pd metal plates out on the cathode in the presence of deuterium gas. At the end of these experiments, tracks were observed along the entire length of the cathode. The density of tracks was greater than that obtained for the Pd wire experiments indicating that the nanostructures created as the result of Pd/D co-deposition exhibit greater activity than bulk Pd. Microscopic examination of the tracks obtained as the result of Pd/D co-deposition shows that the tracks are either circular or elliptical in shape. When focused on the surface of the detector, the tracks are dark in color. Focusing deeper inside the Pd/D co-deposition tracks reveals bright spots attributable to the tips of the track cones. When backlit, the tips of the conical tracks act like lenses and show up as bright spots. These features are consistent with what is observed for tracks obtained when the CR-39 detectors are exposed to alpha sources such as ^{241}Am or depleted uranium.

A series of control experiments were done to show that the tracks obtained in the CR-39 as the result of Pd/D co-deposition were not due to either mechanical or chemical damage [18]. No tracks were observed when CR-39 was placed in contact with the cell components and plating solution indicating that the tracks were not the result of radioactive contamination of the cell, cathodes, polyethylene support structures, heat shrink, or plating solution. Experiments were conducted in the absence of $PdCl_2$. No tracks were observed indicating that the tracks observed in the Pd/D co-deposition experiments could not be due to the impingement of D_2 gases on the surface of the plastic. Experiments were conducted in which the $PdCl_2$ was replaced with $CuCl_2$. For both the $PdCl_2$ and $CuCl_2$ systems, oxygen and chlorine gas evolution occurs at the anode and a metal plates out in the presence of deuterium gas at the cathode. While metallic palladium absorbs deuterium atoms, copper does not. Tracks were observed in the CR-39 used in the palladium electrodeposition but not with copper. These experiments indicate that the tracks are not due to chemical reaction of the CR-39 with either D_2, O_2, or Cl_2 gases. Furthermore, since both the Pd and Cu deposits are dendritic, the tracks observed in the Pd system are not the result of dendrites piercing into the CR-39 detectors or to localized production of hydroxide ions that etch into the plastic. Pd/D co-deposition experiments were also conducted in H_2O. While tracks were observed in the light water system, the density of tracks was at least four orders of magnitude less than was observed in the heavy water system. Since the natural abundance of deuterium in light water is 0.015%, it is possible that the tracks observed in the light water experiments could actually be due to Pd/D interactions.

In this communication, the results of spacer experiments using 6 μm Mylar film between the cathode and the CR-39 detector are discussed. These spacer experiments were done to determine the energy of the particles formed during Pd/D co-deposition. The tracks were also subjected to analysis using the TRACK_TEST modeling program developed by Nikezic and Yu [20,21]. The effect of water on the energetics of charged particles is also discussed.

2 Experimental

2.1 Materials

Palladium chloride (Aldrich), lithium chloride (Mallinckrodt), deuterated water (Aldrich), sodium hydroxide (Baker), 0.25 mm diameter gold wire (Aldrich), 0.5 mm diameter silver wire (Aldrich), and 0.25 mm diameter platinum wire (Aldrich) were used as received. CR-39 detectors (Fukuvi), rectangular in shape with dimensions of 1 cm × 2 cm × 1 mm, were obtained from Landauer and used as received. Prior to using the CR-39 detector in an experiment, one corner of the detector was exposed to an ^{241}Am source. This is used as an internal standard to account for variability in the CR-39 detectors. By having an internal standard on the same detector used in an experiment assures that both sets of tracks experience identical experimental and etching conditions.

2.2 Cell design

The designs for the cells used in the experiments in which the CR-39 detector was in direct contact with the cathode have been described elsewhere [18]. Figure 1a shows the schematic of the electrochemical cell that was used for the Mylar spacer experiments. The rectangular cells (Ridout Plastics) were made of butyrate. A laser was used to cut a square hole in one side of the rectangular cell. A silicone-based cement was used to epoxy a 6 μm thick Mylar film

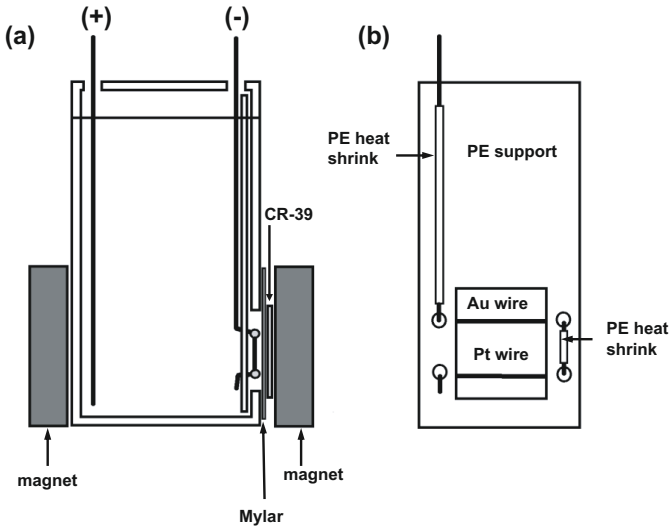

Fig. 1. (a) Schematic of the electrochemical using a 6 μm thick Mylar film between the cathode and the CR-39 detector. (b) Schematic of the cathode comprised of 0.25 mm diameter Au and Pt wires connected in series. PE = polyethyene.

over the hole. Figure 1b is a schematic of the cathode. A square hole is cut inside a polyethylene support. The square hole of the polyethylene support lines up with the hole in the cell. A Pt wire and Au wire were mounted on the polyethylene support in such a manner that, when the cathode is placed in the cell, the Au and Pt wires are in direct contact with the Mylar film. Polyethylene heat shrink is used to provide a pressure contact between the Au and Pt wires. The anode consisted of platinum wire mounted on a polyethylene support [18]. The anode and cathode were connected to a potentiostat/galvanostat (PAR model 363). As shown in Figure 1a, the CR-39 detector is placed outside the cell and is in contact with the Mylar film. Two 1 in × 1 in × 0.25 in permanent NdFeB magnets (Dura Magnetics), on either side of the cell, hold the CR-39 detector in place. The strength of the magnetic field is approximately 2500 Gauss.

2.3 Charging procedure

Typically 20–25 mL solution of 0.03 M palladium chloride and 0.3 M lithium chloride in deuterated water is added to the cell. Palladium is then plated out onto the cathode substrate using a charging profile of 100 μA for 24 h, followed by 200 μA for 48 h followed by 500 μA until the palladium has been plated out. This charging profile assures good adherence of the palladium on the electrode substrate. After the palladium has been electrochemically plated out, the cathodic current is increased to 1 mA for 2 h, 2 mA for 6 h, 5 mA for 24 h, 10 mA for 24 h, 25 mA for 24 h, 50 mA for 24 h, 75 mA for 24 h , and 100 mA for 24 h. The area the Pd plates out is typically on the order of 0.4 cm^2. Given the amount of plating solution placed in the cell, the density of Pd is estimated to be 9×10^{20} to 1.1×10^{21} Pd atoms cm^2 .

2.4 Etching of CR-39 and analysis of etched CR-39 detector

When the experiment was terminated, the cell was disassembled and the CR-39 detector was etched in an aqueous 6.5 N sodium hydroxide solution at 65–72 °C for 6 h.

Microscopic examination of the etched CR-39 detectors was done using an Eclipse E600 epifluorescent microscope (Nikon) and CoolSnap HQ CCD camera (Photometrics). Magnifications of 20× to 1000× were used.

Scanning of the CR-39 detectors was done using an automated scanning track analysis system to obtain quantitative information on the pits produced in the CR-39. The system has a high quality microscope optical system (Nikon cfi series) operating at a magnification high enough to discriminate between tracks and background. The images obtained are then analyzed by the proprietary software. The software makes 15 characteristic measurements of each feature located in the image to provide reliable discrimination between etched tracks and background features present on or in the plastic detectors. These measurements include track length and diameter, optical density (average image contrast) and image symmetry. Based upon the measured properties of a feature, the software of the automated scanning system determines whether or not the measured features are consistent with that of an energetic particle. The software ignores overlapping tracks.

2.5 SEM analysis of Pd/D Co-deposited films

Experiments were conducted using gold foil as the cathode substrate. At the end of these experiments, SEM analysis of the Pd deposits on the Au foil was done using a Hitachi model S-4700 system.

3 Results and discussion

3.1 Results of mylar spacer experiments

When a charged particle traverses inside CR-39, it leaves behind an ionization trail that is more sensitive to chemical etching than the rest of the bulk. Upon treatment with a chemical etching agent, tracks remain as holes or pits. Figure 2a shows representative tracks in a CR-39 detector that have been obtained as the result of a Pd/D co-deposition experiment conducted with the cathode in direct contact with the detector. In Figure 2a, dark, small and large pits, as well as circular and elliptical pits are observed on the surface of the detector. When the microscope optics are focused on the bottom of the tracks, Figure 2b, bright spots are observed inside the pits. As discussed *vide supra*, the bright spots are due to the tips of the cones acting like lenses when the detector is backlit. The size of the pit created by the energetic particle in the SSNTD depends upon the particle's size, energy, and charge. The implication is that, by measuring the size of the track, it should be possible to identify the particle that created the track and to determine its energy. Calibration curves

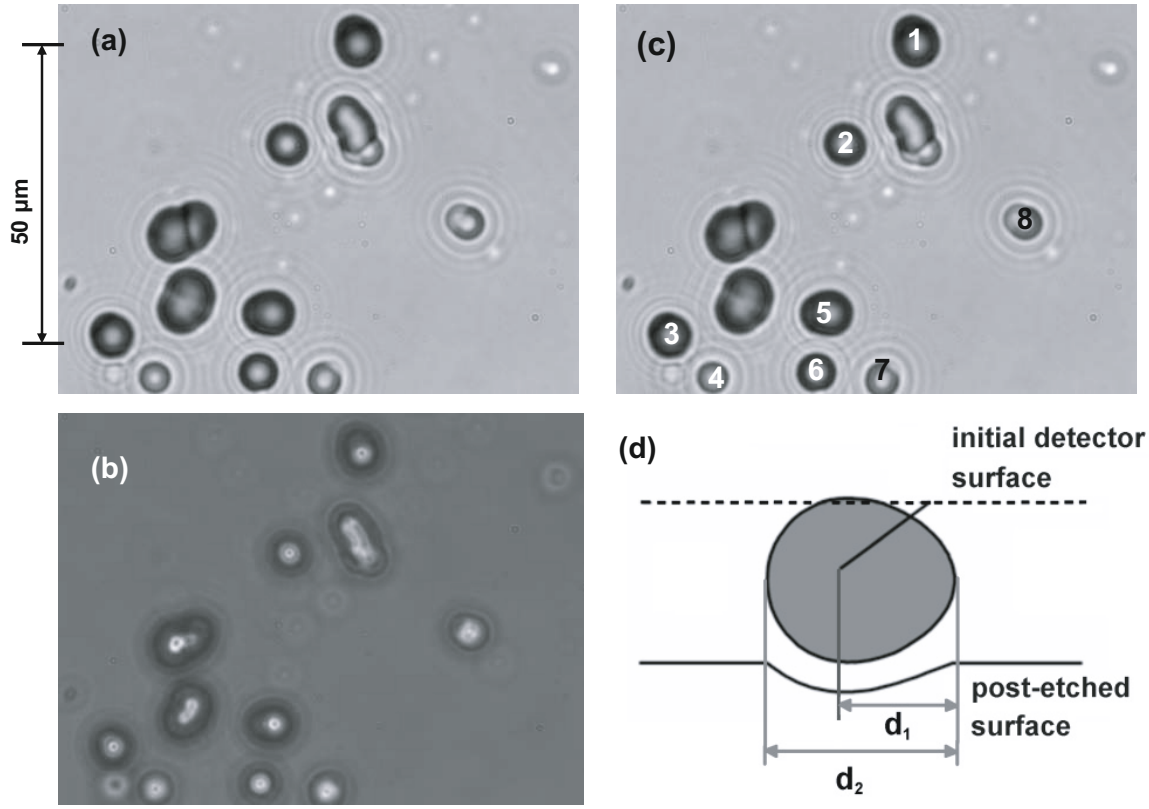

Fig. 2. Images of tracks in CR-39 created as the result of a Pd/D co-deposition reaction. Ag wire, no external field experiment, 1000× magnification. The detector is in contact with the cathode. (a) Focus on the surface of the CR-39. (b) Overlay of two images taken at two different focal lengths (surface and the bottom of the tracks). (c) Numbers 1–8 indicate the tracks that were modeled. Table 1 summarizes the parameters that were measured. Table 2 summarizes the results of the modeling. (d) Results of computer modeling track 1 indicated in (c), This is the shape of the track obtained for a 1.3 MeV alpha particle hitting the CR-39 detector at a 35° angle after 6 h of etching at an etch rate of 1.25 μm h^{-1}.

can be obtained by exposing CR-39 detectors to known sources. This has been done in the ICF community. They have prepared calibration curves by exposing CR-39 detectors to cyclotron generated, collimated, mono-energetic particle beams [1]. These calibration curves show that it is not possible to differentiate alphas, protons, and tritons with energies less than 1 MeV. Also the energetic particles created using a particle beam, under ideal conditions, do not behave in the same fashion as energetic particles emitted from a source such as ^{241}Am or depleted U. Such sources emit energetic particles anisotropically. Figure 3a shows the size distribution of the tracks obtained for a CR-39 detector that has been exposed to an ^{241}Am source that emits 5.6 MeV alpha particles. In this exposure, the separation between the source and the CR-39 detector was ∼2 mm. While the tracks obtained for the charged particles created using a particle beam exhibit a narrow size distribution because the beam is collimated, the same is not true of the size distribution of the ^{241}Am-generated tracks. Figure 3a shows that the major axis for the tracks obtained for the ^{241}Am alphas ranges in size between 8 and 28 μm. This size distribution is the result of alpha scattering within the source as well as within the medium they are traversing, which is a function of the distance between the source and the detector. The greater the distance between the source and the detector, the greater the energy loss and the more oblique the particle's angle of incidence as it enters the CR-39 detector. This will result in the formation of elliptical tracks, as illustrated in the plot of minor axis vs. major axis, Figure 3b. Alpha particles that hit normal to the surface will leave a circular pit whose minor axis approximately equals the major axis. If the angle of incidence is oblique, the resultant track will be elliptical and the major axis will be larger than the minor axis.

As reported earlier [18], the particles produced during Pd/D co-deposition also exhibit a size distribution. If the resultant tracks are caused by protons, tritons, or alphas with a range of energies, there will be considerable overlap among the size distributions of those particles. Consequently calibration curves cannot be used to determine the species that created the tracks or their energies. Placing spacer materials between the cathode and the detector provides a better means of characterizing the energetic particles. As discussed *vide supra*, Lipson et al. [17] used Al and Cu spacers in their experiments to determine the energies of the particle formed. In Pd/D co-deposition experiments, Al and Cu spacers cannot be used as the Pd ions in the plating solution will electrolessly replace the Al and Cu. Instead 6 μm Mylar film was placed between the

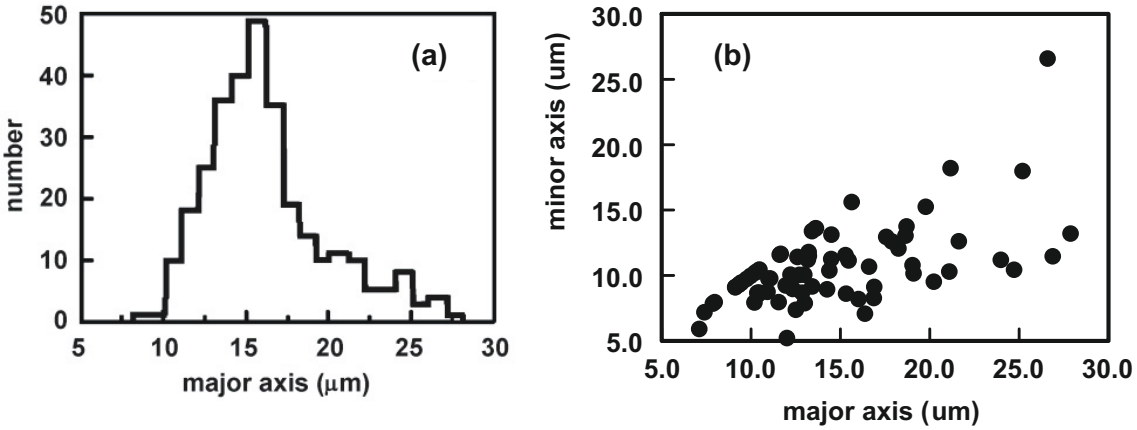

Fig. 3. Quantitative analysis of tracks obtained by exposing a CR-39 detector to an ^{241}Am alpha source for 10 s ($N = 136$ tracks). (a) Size distribution of tracks. (b) Plot of track minor axis vs. major axis.

cathode and the CR-39 detector. The cell configuration shown in Figure 1a was used. Both the Au and Pt wires of the cathode were in direct contact with the Mylar firm. At the completion of the experiment, the CR-39 detector was etched. Microscopic examination of the detector indicated that there was a significant drop in the number of tracks. For the experiments conducted with the cathode in direct contact with the CR-39 detector, the number of tracks was so high that the amount of space allotted by the software of the automated scanner to record the track properties was overflowed. As a result, the detectors had to be scanned in a piecemeal fashion. This was not the case of the spacer experiments. The automated scanner was able to scan the entire surface of the detector in a single session. It is estimated that, by placing a 6 μm thick Mylar film between the detector and the cathode, ~90% of the energetic particles are blocked. Linear energy transfer (LET) curves were used to estimate the energies of the particles that reached the CR-39 detector. The LET curve for Mylar was calculated using the SRIM-2003.26 code of Ziegler and Biersack [22]. Based upon the Mylar LET curve, 6 μm thick Mylar cuts off <0.45 MeV protons, <0.55 MeV tritons, <1.40 MeV ^{3}He, and <1.45 MeV alphas. However, as indicated above, this is the energy of the particle when it reaches the CR-39 detector. In order to reach the detector, the energetic particle has to traverse through a water layer between the cathode and Mylar as well as the Mylar film itself. The effect of water on the energetics of the charged particles will be discussed *vide infra*.

Figure 4a shows an image of the tracks obtained as the result of a Mylar experiment using Pd/D co-deposition. This image was taken by the automated scanning system. As can be seen in the microphotograph, there are large and small tracks as well as both circular and elliptical tracks. The spatial distribution of the tracks is shown in Figure 4b. When the Pd plates out on the Au and Pt wires, the deposit extends several mm away on either side of the wires. From the spatial distribution shown in Figure 4b, it can be seen that the density of tracks is higher where the cathode wires were in contact with the Mylar. The density of tracks is higher for the Au wire. It is not known if this is due to higher activity of the Pd deposit attached to the Au wire or if the Au wire had better contact with the Mylar film. The size distribution of the tracks on the CR-39 detector is shown in Figure 4c. There are two populations of tracks. The majority of the tracks fall between 2–3 μm. The second population of tracks extends from 4 μm in diameter all the way out to 40 μm. Figure 4d shows a plot of the minor axis vs. major axis. This plot is used to determine the degree of ellipticity of the tracks. This plot indicates that the majority of the tracks are circular in shape. The cause of this is discussed *vide infra*. Given the disparity in the size distribution of the two populations of tracks shown in Figure 4c, they are probably due to different particle types. Based upon their size, the population of tracks between 2–3 μm is tentatively assigned to >0.45 MeV protons and/or >0.55 MeV tritons. The second population of tracks is tentatively assigned to >1.40 MeV ^{3}He and/or >1.45 MeV alphas. This estimate of the particle energies does not take into account the impact of a water layer that the particles will have to traverse before they get to the Mylar film.

3.2 Effect of water on particle energy

In the conventional Pd/D experiment that yielded the tracks shown in Figure 2, the CR-39 detector is in direct contact with the cathode. In this experimental configuration, the detector and the cathode are immersed in the electrolyte. During electrolysis, Pd plates out on the surface of the cathode. Figure 5a shows a SEM of the metal deposit that is formed as the result of Pd/D co-deposition. The metal deposit is not smooth and exhibits a cauliflower-like morphology that will trap pockets of water. Consequently, the particles have to traverse a film of water before they reach the CR-39 detector. Because of the cauliflower structure of the metal deposit, the thickness of the water film between the detector and the Pd deposit will vary. The presence of water will slow the particles down causing them to lose energy.

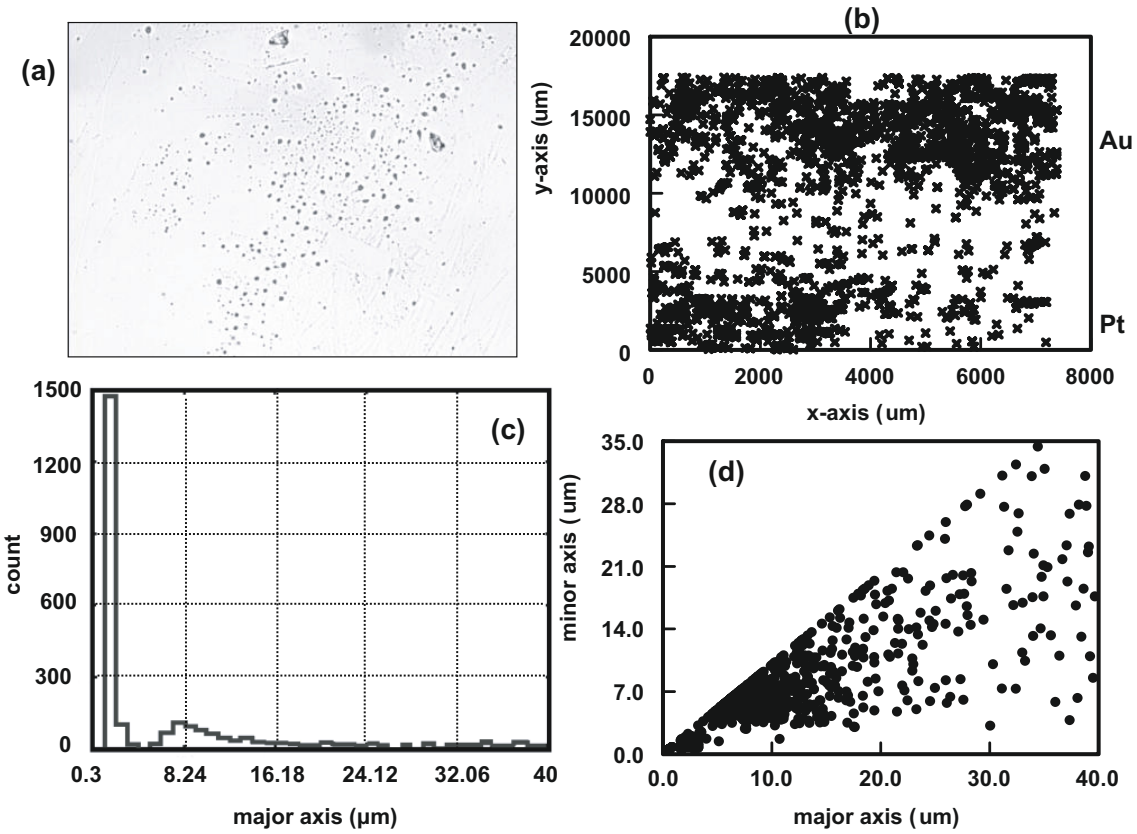

Fig. 4. Summary of 6 μm Mylar spacer experiments. Figure 1 shows the schematics of the electrochemical cell and cathode. (a) Photomicrograph of tracks in CR-39 obtained on the CR-39 detector. 200× magnification (field of view is 500 μm by 600 μm). Quantitative analysis of tracks obtained ($N = 2387$ tracks): (b) spatial distribution of the tracks on the CR-39 detector. Spatial orientation of the Au and Pt wires is indictated. (c) Size distribution of the tracks. (d) Plot of track minor axis vs. major axis.

To determine the effect of water on the energy of the particles, LET curves were calculated using the SRIM-2003.26 code of Ziegler and Biersack [22]. Figure 5b shows LET curves, calculated as a function of water thickness, for alphas, ^{3}He, protons, and tritons. The LET curves indicate that the impact of the water layer on the energies of the charged particles is greatest for alphas and ^{3}He. Both alphas and ^{3}He are more massive than protons and tritons. The charge on the alphas and ^{3}He is +2 while that for protons and tritons is +1. These calculations indicate that the magnitude of the energy loss as a particle traverse through water depends upon its mass and charge. In the case of the Mylar-spacer experiments, the emitted particles have to traverse the water film and the Mylar before they reach the CR-39 detectors. Because of the morphology of the Pd deposit, the thickness of the water layer will vary. Taking into account the impact of the 6 μm thick Mylar film on the particles, for a water thickness varying between 0 and 10 μm, it is estimated that the majority of the particles formed as a result of Pd/D co-deposition are <0.45–0.97 MeV protons, <0.55–1.25 MeV tritons, <1.40–3.15 MeV ^{3}He and/or <1.45–3.30 MeV alphas. The estimated energies of the alpha particles are supported by computer modeling of the tracks as discussed below.

3.3 Simulating the effect of water on the energetics of charged particles

Figure 6 shows tracks observed as the result of Pd/D co-deposition experiments in which the cathode was in direct contact with the detector. These images were taken in an area away from the cathode where the density of tracks was less. The observed tracks are mostly circular in shape. There are some elliptically shaped tracks as indicated by arrows in the photomicrographs, Figure 6. Figure 6b shows the presence of small, very shallow tracks. No torpedo-shaped tracks are observed. The shapes of these smaller tracks are shown in better detail at higher magnification, Figures 6c and 6d.

To obtain a better understanding of the impact traversing through water has on the energetics of a charged particle, a series of experiments were conducted in which the thickness of the Mylar film between the CR-39 detector and ^{241}Am alpha source was varied. Specifically, sheets of Mylar film were placed between CR-39 detectors and the source. The Mylar layer thicknesses between the detector and source were 6, 12, 18, and 24 μm. Figure 7 summarizes the results of those experiments. The left hand side shows the photomicrographs obtained when the Mylar is between the detector and the ^{241}Am source while

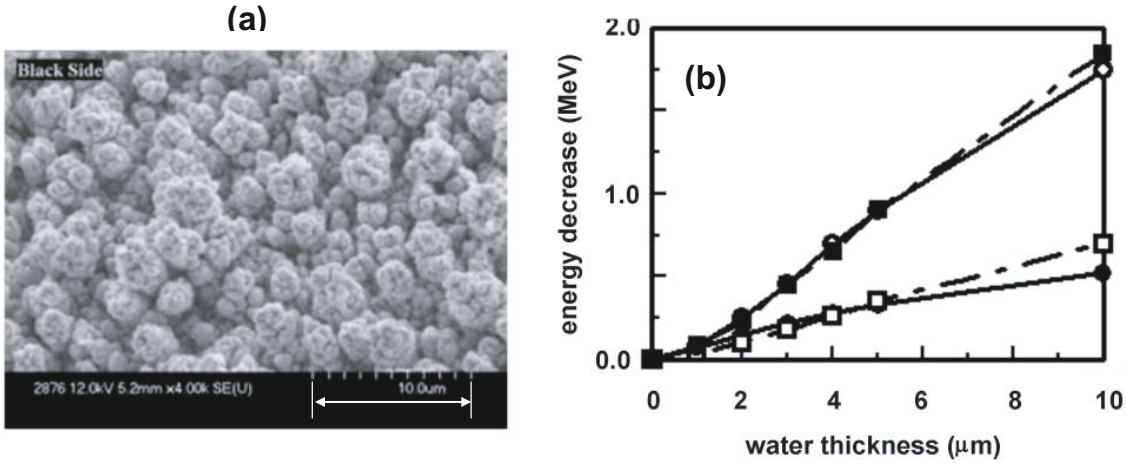

Fig. 5. (a) SEM image of the Pd film deposited on a Au foil. This image shows the cauliflower morphology of the Pd deposit created as a result if Pd/D co-deposition. (b) LET curves showing the decrease in energy as a function of thickness of the water film for alphas (■), ^{3}He (○), tritons (□), and protons (●).

the right hand side shows photomicrographs of tracks resulting from ^{241}Am alphas traversing through ∼ 1 mm air.

Figure 7a shows the results obtained for the ^{241}Am alpha particles traversing 6 μm of Mylar. The most notable difference between the right and left images is that small, narrow, elliptical tracks, like those indicated by arrows in the right hand images in Figure 7, are not observed in the left image. These small, narrow, elliptical tracks are caused by alpha particles that hit the detector at a very oblique angle. These particles are not energetic enough to go through 6 μm of Mylar. When 12 μm of Mylar is placed between the detector and source, fewer torpedo shaped tracks are observed, Figure 7b. Also, compared to the tracks obtained in the absence of Mylar (right hand side), the tracks on the left hand side are visibly larger. Placing 18 μm of Mylar between the detector and source, no torpedo shaped tracks are observed, Figure 7c left hand side. The tracks are primarily circular, oval, or tear-drop in shape. Some very small, circular, shallow tracks, like those seen in Figure 6, are also observed in Figure 7c left hand side. Even fewer tracks are observed when 24 μm of Mylar are placed between the detector and source, Figure 7d left hand side. A greater number of small, circular, shallow tracks are also observed.

The tracks shown in the left hand side photomicrographs shown in Figure 7c and 7d more closely resemble the Pd/D generated tracks shown in Figure 6. The reduced number of elliptical tracks in Figure 6 and Figures 7c and 7d, left hand side, indicate that particles traveling at ∼ 90° angle have sufficient energy to get through the water layer and Mylar to impact the detector. Particles traveling at oblique angles are blocked. The LET curves showing the decrease in energy as a function of thickness of the Mylar film for alphas and protons are shown in Figure 8a. In the case of alpha particles, the LET curve indicates that 6, 12, 18, and 24 μm thick Mylar will block 1.45, 2.75, 3.58, and 4.41 MeV alphas, respectively. The alpha particles emitted by the ^{241}Am source have an energy around 5.6 MeV. Consequently, the alpha particles getting through 18 and 24 μm of Mylar have energies on the order of 2.02 and 1.19 MeV respectively. These energies are in agreement with the energies estimated for the particles generated as the result of Pd/D co-deposition as discussed *vide supra*.

Figures 8b and 8c show tracks obtained when 24 μm of Mylar were placed between the CR-39 detector and the ^{241}Am source. The track shown in Figure 8b resembles track number 8 in Figure 2c as well as the elliptical tracks (indicated by arrows) shown in Figure 6c. In Figure 8c, the track indicated by an arrow resembles track number 7 in Figure 2c. The other three tracks are similar in shape to tracks number 2 and 4 in Figure 2c.

3.4 Computer modeling of the tracks

As discussed *vide supra*, the ionization trail created by the energetic particle traversing through a CR-39 detector is more sensitive to chemical etching than the rest of the bulk. A thorough discussion on the formation and growth of tracks as a function of etching time can be found in a review written by Nikezic and Yu [23]. Based upon their work, Nikezic and Yu have developed a computer program, TRACK_TEST, that calculates track parameters, such as the lengths of the major and minor axes and the track depth [20,21]. The computer program also plots the profile for the etch pit in the SSNTD. The executable program is freeware and can be downloaded from the City University of Hong Kong Trackology Research website [24]. When using TRACK_TEST, the input parameters are particle energy, incident angle, etch rate, and etch time. For the CR-39 detectors used in these experiments, the detector was etched for 6 h. From micrometer measurements as a function of time, the etch rate was determined to be 1.25 μm h^{-1}. In the program, there are three forms of the track etch rate function available for use. These three forms exist because the quality of the CR-39 detectors varies between different manufacturers.

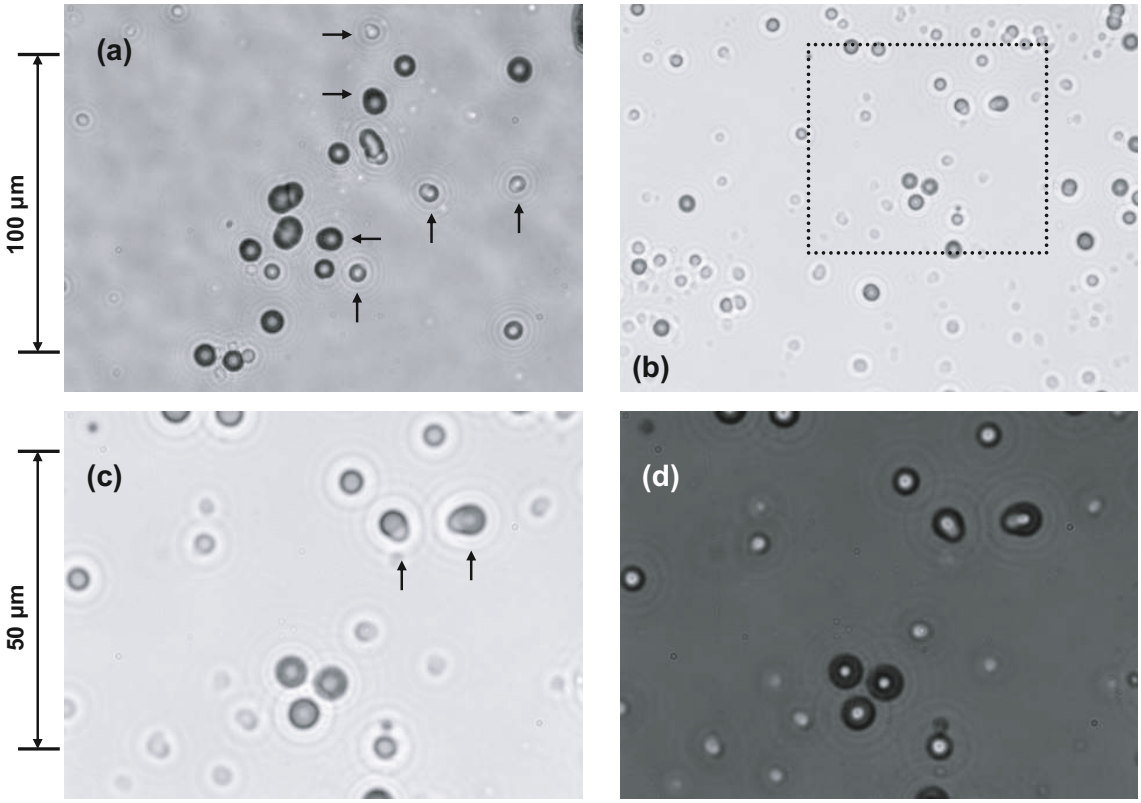

Fig. 6. Photomicrographs of tracks resulting from Pd/D co-deposition. The detector is in contact with the cathode. No external field was applied. (a) Pd is plated on a Ag wire. Magnification was 500×. A higher magnification of this field of view is shown in the photomicrograph in Figure 2a. (b) Pd is plated on a Au.wire cathode. Magnification was 500×. (c) Same field of view as Figure 6b (boxed area) but at a magnification of 1000×. Focus is on the surface of the CR-39. (d) Same field of view as Figure 6c. This photomicrograph is an overlay of two images taken at two different focal lengths (surface and bottom of the tracks). Arrows indicate elliptical tracks.

There are even batch variations in the CR-39 detectors from a given manufacturer. It is up to the user to determine which track etch rate function optimally describes the etching behavior of the detectors being used. This is best done by using all three track rate functions to model tracks generated by a source of known energy and determining which equation gives the best fit. By modeling ^{241}Am alpha tracks in the CR-39 detectors, it was determined that the optimum track rate function for the Fukuvi CR-39 detectors used in these experiments is [25]:

$$V_T = V_B \left(e^{(-a_1 x + a_4)} - e^{(-a_2 x + a_3)} + e^{a_3} - e^{a_4} + 1 \right), \quad (1)$$

where V_T and V_B refer to the rates of etching the track and the bulk respectively and x is the residual range of the alpha particle. The coefficients that gave the best fit between the actual and calculated ^{241}Am alpha tracks are $a_1 = 0.1$, $a_2 = 1$, $a_3 = 1.27$, and $a_4 = 1$. Because we do no have access to a proton source, it was not possible to determine the track etch rate function and coefficients that describe energetic proton tracks. Consequently, the modeling of the Pd/D generated tracks assumes all tracks in the CR-39 detectors are due to alpha particles.

The TRACK_TEST program was used to model the eight, solitary tracks indicated in Figure 2c. As discussed *vide supra*, these tracks were generated using a conventional Pd/D co-deposition experiment where the cathode is in direct contact with the CR-39 detector. The major (M) and minor (m) axes were measured and are tabulated in Table 1. For an elliptical track, two additional parameters, d_1 and d_2 shown in Figure 2d, were measured and are also tabulated in Table 1. Parameter d_2 is equivalent to the major axis while d_1 is the distance between the back edge of the track and the endpoint of the particle path. In Figure 2b, the bright spots inside the tracks indicate the endpoints of the particles.

Using equation (1) in the TRACK_TEST program, track 1 in Figure 2c was modeled. This track has an elliptical shape indicating that the particle has entered the surface of the CR-39 detector at an oblique angle. Computer modeling shows that a 1.3 MeV alpha particle hitting the surface of the CR-39 at a 35^o angle will cause a track with a similar elliptical shape, Figure 2d. The calculated minor and major axes are tabulated in Table 2 as well as the d_1 and d_2 parameters. The measured values tabulated in Table 1, within the uncertainties, are in agreement with the calculated values in Table 2 obtained using the model. This is further emphasized by comparing the measured and calculated ratio of the minor vs. major axis of the track, $R_{m/M}$, and ratio of d_1 and d_2, $R_{d1/d2}$,

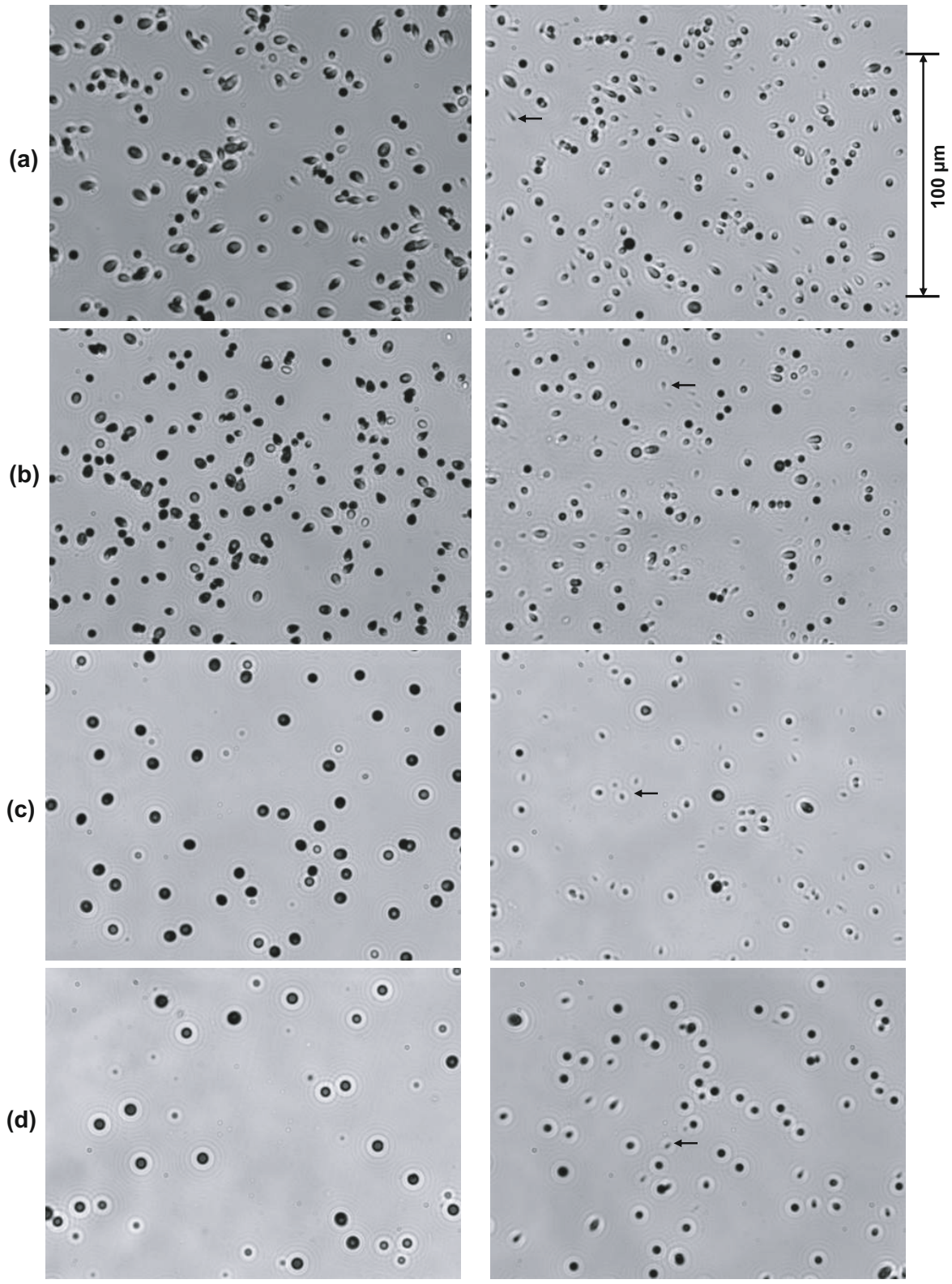

Fig. 7. Photomicrographs obtained by varying the thickness of the Mylar layer between the CR-39 detector and the ^{241}Am source. Left hand side photomicrographs were obtained with the Mylar layer between the detector and the source. The right hand side photomicrographs are of the internal standard, described *vide supra*, in which no Mylar layer was between the detector and the source. Film thicknesses were (a) 6 μm, (b) 12 μm, (c) 18 μm, and (d) 24 μm. Arrows in the right-hand side photomicrographs indicate small, elliptical tracks that have entered the CR-39 detector in an oblique angle. To obtain the photomicrograph for the 24 μm thick Mylar layer, the detector was exposed to the ^{241}Am source for 30 s. All others were obtained using a 10 s exposure to the ^{241}Am source.

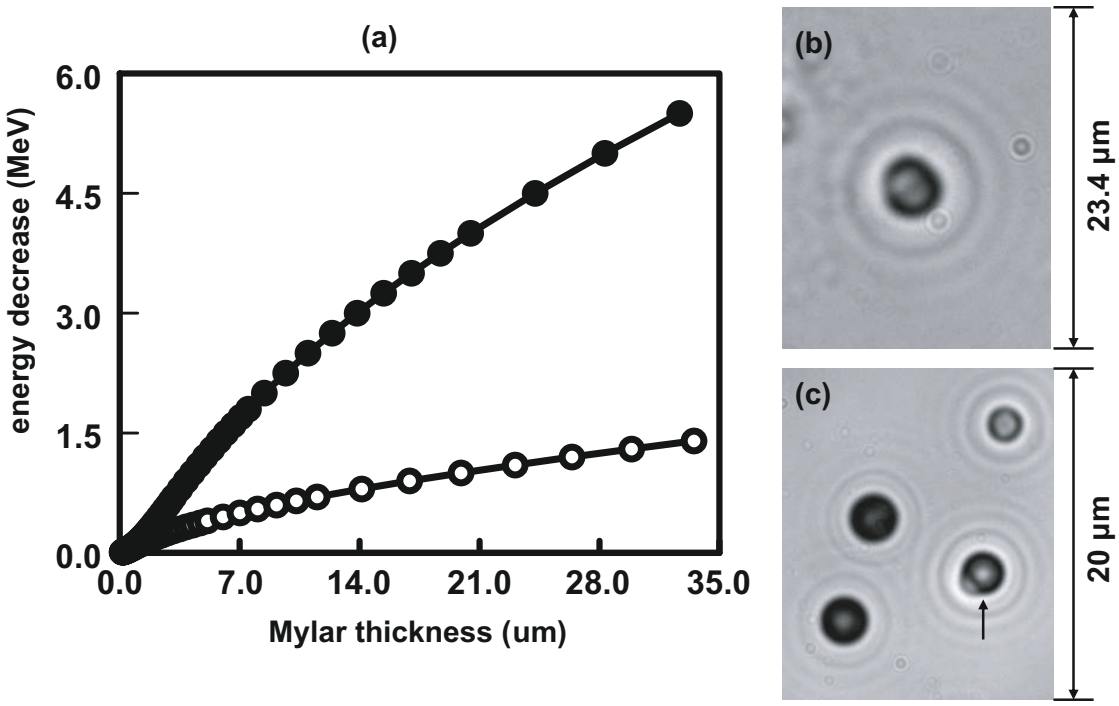

Fig. 8. (a) LET curves showing the decrease in energy as a function of thickness of the Mylar film for (•) alphas and (○) protons. Elliptical tracks obtained when there is 24 μm thick Mylar between the detector and the source where (b) is similar to track number 8 shown in Figure 2c and (c) the track indicated by an arrow is similar to track number 7 in Figure 2c.

tabulated in Tables 1 and 2. These ratios are, within the experimental uncertainties, in agreement with each other.

Tracks 2 through 8 were also subjected to computer analysis. In Table 2, the energy and angle of incidence used in the calculations are indicated. The measured and calculated values of the major and minor axes as well as the d_1 and d_2 parameters for elliptical tracks are summarized in Tables 1 and 2. Within the experimental uncertainties, the measured and calculated values are in agreement.

Another parameter calculated by the TRACK_ETCH program is track depth. The calculated track depth for all eight tracks indicated in Figure 2c are tabulated in Table 2 along with the other calculated parameters that describe the track. While it was not possible to directly measure the depth of the tracks, using the photomicrograph shown in Figure 2b, it is possible to compare the relative depths of the tracks. The photomicrograph in Figure 2b is an overlay of two images obtained at two focal lengths – the surface of the CR-39 and the bottom of the pits. However, it can be seen that the bright spots of the tracks are not all in focus. This is because the bright spots occur at different depths. The deepest tracks are the ones with the sharper focus. These would be tracks 1 and 5. As shown in Table 2, these tracks are the deepest ones with depths of 1.39 and 1.42 μm, respectively. The shallowest tracks would be the most out of focus. In Figure 2b, the tracks most out of focus are tracks 4, 7, and 8. As shown by the calculated track depths summarized in Table 2, tracks 4, 7, and 8 are the shallowest. In Figure 2b, tracks 2, 3, and 6 show the bright spot but it is not as tightly focused as the bright spots observed for tracks 1 and 5. This suggests that these tracks are shallower than tracks 1 and 5 but deeper than tracks 4, 7, and 8. This supposition is in agreement with the calculated track depths for tracks 2, 3, and 6 tabulated in Table 2.

Assuming that tracks 1–8 shown in Figure 2c are attributable to alpha particles, modeling using the TRACK_ETCH program indicates that the alpha particles have energies ranging between 0.15 and 1.3 MeV. However, it needs to be emphasized that the alpha particle energies summarized in Table 2 are the energies of the particles once they impact the CR-39 detector. As discussed *vide supra*, the particles will traverse a layer of water that will slow the particles down before they reach the CR-39 detector. The thicker the water layer, the lower the energy of the particle that is registered on the detector. Assuming water thicknesses between 0 and 10 μm, the particle whose energy was 0.15 MeV by the time it reached the detector, had at its birth an energy between 0.15–2.00 MeV. Likewise the particle whose energy was 1.30 MeV by the time it reached the detector, had at its birth an energy between 1.30–3.15 MeV, depending upon the thickness of the water layer the particle traversed. The track modeling is in agreement with the 6 μm Mylar spacer experiments described *vide supra*.

3.5 Discussion on the origins of the charged particles

Are the particle emissions observed in these experiments due to DD fusion products that have undergone energy loss or are they due to a new effect that is different from DD fusion products? In plasma fusion, the primary

Table 1. Measured track parameters for the Pd/D-generated tracks shown in Figure 5a. Etch time is 6 h and etch rate is 1.25 μm h^{-1}.

Track [a] number	Major axis (μm)	Minor axis (μm)	$R_{m/M}$ [b]	d_1^c (μm)	d_2^c (μm)	R_{d_1/d_2} [d]
1	9.36 ± 0.19	7.68 ± 0.19	0.82	5.34 ± 0.19	9.36 ± 0.19	0.57
2	7.49 ± 0.19	7.49 ± 0.19	1	—	—	—
3	7.87 ± 0.19	7.30 ± 0.19	0.93	4.12 ± 0.19	7.87 ± 0.19	0.52
4	5.62 ± 0.19	5.62 ± 0.19	1	—	—	—
5	9.06 ± 0.19	7.87 ± 0.19	0.87	5.24 ± 0.19	9.06 ± 0.19	0.58
6	7.12 ± 0.19	7.12 ± 0.19	1	—	—	—
7	7.49 ± 0.19	6.40 ± 0.19	0.85	4.96 ± 0.19	7.49 ± 0.19	0.66
8	7.12 ± 0.19	5.43 ± 0.19	0.76	5.16 ± 0.19	7.12 ± 0.19	0.72

[a] Tracks are designated in Figure 2c, [b] $r_{m/M}$ is the ratio of the minor axis (m) and the major axis (M), [c] refer to Figure 5b for the d_1 and d_2 parameters, [d] R_{d_1/d_2} is the ratio of d_1 and d_2.

Table 2. Calculated track parameters. Etch time is 6 h and etch rate is 1.25 μm h^{-1}.

Track [a] number	Energy (MeV)	Incident angle (°)	Major axis (μm)	Minor axis (μm)	$R_{m/M}^b$	Track depth (μm)	d_1^c (μm)	d_2^c (μm)	R_{d_1/d_2} [d]
1	1.3	35	9.32	7.68	0.82	1.39	5.59	9.32	0.60
2	0.32	90	7.46	7.46	1	1.12	—	—	—
3	0.7	45	7.80	7.39	0.95	1.15	4.28	7.80	0.55
4	0.15	90	5.74	5.74	1	0.62	—	—	—
5	1.18	37.5	9.09	7.83	0.86	1.42	5.31	9.09	0.58
6	0.28	90	7.14	7.14	1	1.01	—	—	—
7	0.825	35	7.35	6.51	0.89	0.88	5.11	7.35	0.70
8	1	27.5	7.05	5.52	0.78	0.63	5.36	7.05	0.76

[a] Tracks that are modeled are designated in Figure 2c, [b] $R_{m/M}$ is the ratio of the minor axis (m) and the major axis (M), [c] refer to Figure 5b for the d_1 and d_2 parameters, [d] $R_{d1/d2}$ is the ratio of d_1 and d_2.

reactions that occur in DD fusion are [1]:

$$\mathrm{D} + \mathrm{D} \rightarrow \mathrm{T}\,(1.01\ \mathrm{MeV}) + p\,(3.02\ \mathrm{MeV}) \quad (2)$$

$$\mathrm{D} + \mathrm{D} \rightarrow n\,(2.45\ \mathrm{MeV}) + {}^3\mathrm{He}\,(0.82\ \mathrm{MeV}). \quad (3)$$

The secondary reactions that occur in plasma fusion are:

$$\mathrm{D} + \mathrm{T}\,(\leqslant 1.01\ \mathrm{MeV}) \rightarrow \alpha\,(6.7{-}1.4\ \mathrm{MeV}) + n\,(11.9{-}17.2\ \mathrm{MeV}) \quad (4)$$

$$\mathrm{D} + {}^3\mathrm{He}\,(\leqslant 0.82\ \mathrm{MeV}) \rightarrow \alpha\,(6.6{-}1.7\ \mathrm{MeV}) + p\,(12.6{-}17.5\ \mathrm{MeV}). \quad (5)$$

The size distribution of tracks obtained for Pd/D co-deposition experiments conducted with a 6 μm thick Mylar film between the CR-39 detector and cathode, Figure 4c, indicates that there are two populations of charged particles. To go through 6 μm Mylar and 0–10 μm water, the energies of the particles observed in the CR-39 detectors are > 0.45-0.97 MeV protons, >0.55–1.25 MeV tritons, > 1.40–3.15 MeV ^{3}He, and >1.45–3.30 MeV alphas. The spacer experiments, simulations done by placing Mylar film between an ^{241}Am source and CR-39 detectors, and track modeling also indicate that the majority of the Pd/D charged particles are <0.45–0.97 MeV protons, <0.55–1.25 MeV tritons, <1.40–3.15 MeV ^{3}He, and <1.45–3.30 MeV alphas. The energies of the particles observed as a result of Pd/D co-deposition are consistent with the energies of the charged particles formed as the result of reactions 2–5. Others have reported detecting neutrons and charged particles resulting from DD fusion, reactions 2 and 3 [15,26,27]. However, we are the first to suggest that secondary fusion reactions, in particular reaction 4, are also occurring inside the Pd lattice. Triple tracks have been observed in CR-39 detectors that were used in Pd/D co-deposition experiments [28]. These triple tracks have been observed in DT fusion reactions and are diagnostic of the ^{12}C$(n, n')3\alpha$ carbon breakup reaction [7–12]. The threshold energy of the neutron to cause the carbon breakup reaction is $\geqslant$9.6 MeV [9].

4 Conclusions

Earlier we reported that pits formed on CR-39 detectors during Pd/D co-deposition exhibited features that were consistent with those observed for tracks of a nuclear origin [18]. Specifically, the Pd/D generated pits are dark in color, circular/elliptical in shape, and have bright centers when focusing deeper in the plastic. A series of control experiments were conducted that indicated that the Pd/D

generated pits did not have either a chemical or mechanical origin. In particular, the observed pits were not due to radioactive contamination of the cell components; or to impingement of the gas bubbles on the surface of the detector; or to chemical attack by D_2, O_2, or Cl_2 gases; or to the metal dendrites piercing into the plastic. More recently we have conducted experiments in which 6 μm Mylar is placed between the CR-39 detector and the cathode. The purpose of these experiments was to characterize the particles emitted during Pd/D co-deposition. By placing a 6 μm thick Mylar film between the cathode and the detector, it was observed that ~90% of the energetic particles are blocked. Using LET curves, a 6 μm thick Mylar film cuts off <0.45 MeV protons, <0.55 MeV tritons, <1.40 MeV ^{3}He, and <1.45 MeV alphas. However, this is the energy of the particle when it reaches the CR-39 detector. It does not take into account the water layer the particle needs to traverse before it reaches the Mylar film. The Pd deposit exhibits a cauliflower like structure. Because of this structure, the particles need to traverse a water layer of varying thickness. Assuming water thicknesses varying between 0 and 10 μm, it is estimated that the majority of the particles formed as a result of Pd/D co-deposition are <0.45–0.97 MeV protons, <0.55–1.25 MeV tritons, <1.40–3.15 MeV ^{3}He, and <1.45–3.30 MeV alphas. The estimated energies of the alpha particles are supported by computer modeling of the tracks using the TRACK_ETCH program developed by Nikezic and Yu [23]. The energies of the particles formed as a result of Pd/D co-deposition are consistent with DD primary and secondary fusion reactions.

This work was funded by the SSC-Pacific ILIR program and JWK Corporation. The authors would like to thank Dr. Gary Phillips, nuclear physicist, retired Naval Research Laboratory, US Navy, Radiation Effects Branch, for calculating the LET curves and for valuable discussions in interpreting the data. They would also like to thank Mr. Steven Krivit of New Energy Times for supplying the cells that were used in the Mylar film experiments and Dr. Ludwik Kowalski, retired from Montclair State University, for suggesting the experiments to vary the thickness of the Mylar film between the detector and the source. Finally, the authors would also like to thank Dr. Jay W. Khim, CEO of JWK Corporation, for funding project GeNiE at JWK International and for his valuable discussions with regards to experiments and data analysis.

References

1. F.H. Séguin, J.A. Frenje, C.K. Li et al., Rev. Sci. Instrum. **74**, 975 (2003)
2. T. Yoshioka, T. Tsuruta, H. Iwano, T. Danhara, Nucl. Instrum. Meth. Phys. Res. A **555**, 386 (2005)
3. S. Szpak, P.A. Mosier-Boss, R.D. Boss, J.J. Smith, Fus. Technol. **33**, 38 (1998)
4. S. Szpak, P.A. Mosier-Boss, F.E. Gordon, Naturwissenschaften **94**, 511 (2007)
5. S. Szpak, P.A. Mosier-Boss, J.J. Smith, Phys. Lett. A **210**, 382 (1996)
6. M.H. Miles, R.A. Hollins, B.F. Bush. J.J. Lagowski, R. Miles, J. Electroanal. Chem. **346**, 99 (1993)
7. A.M. Abdel-Moneim, A. Abdel-Naby, Radiat. Meas. **37**, 15 (2003)
8. A. Aframian, J. Phys. G: Nucl. Phys. **9**, 985 (1983)
9. S.A.R. Al-Najjar, A. Abdel-Naby, S.A. Durrani, Nucl. Tracks **12**, 611 (1986)
10. B. Antolkoviæ, Z. Dolenec, Nucl. Phys. A **237**, 235 (1975)
11. J.K. Pálfalvi, J. Szabó, Y. Akatov, L. Sajó-Bohus, I. Eördögh, Radiat. Meas. **40**, 428 (2005)
12. L. Sajó-Bohus, J.K. Pálfalvi, Y. Akatov et al., Radiat. Meas. **40**, 442 (2005)
13. S.A. Durrani, Radiat. Meas. **43**, S26 (2008)
14. R.A. Oriani, J.C. Fisher, Jpn J. Appl. Phys. **41**, 6180 (2002)
15. A.G. Lipson, B.F. Lyakhov, A.S. Roussetski et al., Fus. Technol. **38**, 238 (2000)
16. A.G. Lipson, A.S. Roussetski, G.H. Miley, E.I. Saunin, in *Tenth Int. Conf. on Cold Fusion, Cambridge, MA, USA, 2003*, http://www.LENR-CANR.org
17. A.G. Lipson, A.S. Roussetski, G.H. Miley, C.H. Castano, in *9th Int. Conf. Cold Fusion, Condensed Matter Nuclear Science* (Tsinghua Univ. Press, Beijing, China, 2002)
18. P.A. Mosier-Boss, S. Szpak, F.E. Gordon, L.P.G. Forsley, Eur. Phys. J. Appl. Phys. **40**, 293 (2007)
19. E. Storms, in *6th Int. Conf. Cold Fusion, Progress in New Hydrogen Energy* (Tokyo Institute of Technology, Tokyo, Japan, 1996)
20. D. Nikezic, K.N. Yu, Comp. Phys. Commun. **174** , 160 (2006)
21. D. Nikezic, K.N. Yu, Radiat. Meas. **37**, 39 (2003)
22. J.F. Ziegler, J.P. Biersack, *The Stopping and Range of Ions in Solids* (Pergamon, New York, 1985)
23. D. Nikezic, K.N. Yu, Mat. Sci. Eng. R. **46**, 51 (2004)
24. http://www.cityu.edu.hk/ap/nru/test.htm
25. C. Brun, M. Fromm, M. Jouffroy et al., Radiat. Meas. **31**, 89 (1999)
26. S.E. Jones, E.P. Palmer, J.B. Czirr et al., Nature **338**, 737 (1989)
27. S.E. Jones, E.P. Palmer, J.B. Czirr et al., J. Nucl. Fus. Energy **9**, 199 (1990)
28. P.A. Mosier-Boss, S. Szpak, F.E. Gordon, L.P.G. Forsley, Naturwissenschaften **96**, 135 (2009)